Full relativistic Atomic Structure Calculations of X-ray Laser radiation from Ne-like Argon

Hamed M. Kandel
Department of Laser Sciences and Interactions, , National Institute of Laser Enhanced Sciences, Cairo University, P.O. Box 12613, Giza, Egypt

Abstract:

Energy levels, transition probabilities and oscillator strengths as well as effective collision strengths were calculated for 89 fine structure energy levels of Ar IX. The data refer to levels belonging to the configurations $(1s^2)\ 2s^2\ sp^6$, $2s^2\ 2p^5\ 3l$, $2s^2\ 2p^5\ 4l$, $2s^1\ 2p^6\ 3l$, and $2s^1\ 2p^6\ 4l$ where l = s,p,d,and f. the atomic structure calculations were carried out by The full relativistic atomic structure program (FAC). The atomic structure data were used to simultaneously solving 89 coupled rate equations for calculations of levels populations as well as gain coefficient of laser transitions between these levels at different plasma temperatures and different electron densities.

Keywords: x-ray laser; transition probabilities; oscillator strengths; gain coefficient; collision strength

Introduction:

X-ray lasers have multi applications in different scientific branches such as photoexcitaion, photoinoization in atomic physics science, electron spectroscopy for chemical Analysis, diagnostics of high-density fusion plasma, photolithography, grating and grid production as well as biological applications such as x-ray microscopy, x-ray diffractometry, and x-ray holography. X-ray lasers were demonstrated for the first time in 1984 in large laboratories from plasma generated by high power lasers [1,2].

X-ray lasers requires highly power pump sources to cover the energy gab between lower and upper laser levels in this very short wavelength region of electromagnetic spectrum (1-30 nm). In last two decades, many efforts were done to produce simple low cost table top x-ray lasers [3-8]. The x-ray lasers are mainly produced from the plasma of highly ionized Neon or Nickel-like ions due the relative stability of this plasma in wide range of temperature and density [9-10].

There are different pumping mechanism for x-ray lasers such as photo excitation, electron collisional excitation, charge transfer, de-electronic recombination and electron collisional recombination pumping [11], a capillary discharge is an example of electron collisional pumping method [3,12].

The electron collisional excitation pumping of the highly ionized atoms is the most favorable pumping technique [13-14]. Neon-like and Nickel-like x-ray lasers were extensively studied [15-23]. In Neon-like ions, scientists studied mostly laser lines due the excitation outer shell 3p electron and the x-ray laser produced mainly from $2p^5 3p \rightarrow 2p^5 3s$ transitions. In 1994, the first Table-top 46.9 nm laser in Ne-like Argon was demonstrated by Rocca [3], however not much work were done to study the capability of producing X-ray laser radiation due to the excitation of the inner-shell 2s electron which gives the chance of obtaining shorter wavelength from the same ion without demanding of highly ionized ions[13-14, 24-27].

In this paper, the atomic structure of Ne-like Ar ion were studied. Firstly, a 89 fine-structure energy levels arising from the configurations $(1s^2)\ 2s^2\ sp^6$, $2s^2 2p^5\ 3l$, $2s^2 2p^5\ 4l$, $2s^1 2p^6\ 3l$, and $2s^1 2p^6\ 4l$ where $l = s,p,d,$ and f were calculated using FAC code which is according to Dirac equation. Weighted Oscillator strengths, rates of spontaneous radiative decay and Collision strengths caused by electron impact excitation are also evaluated in the distorted wave approximation.

Effective collision strengths then calculated by interposing the data resulted from the collision strengths and integrating over Maxwellian distribution at various temperatures. Finally, the laser gain from Ar IX is predicted after solving steady state rate equations for all 89 energy levels simultaneously by our Collisional radiative model. Our model treats the kinetic of the Ne-like charge state in isolation from other ionization stages to calculate the population of each state at different plasma temperature and electron density.

Theory of atomic structure and gain calculations

Energy Levels

The energy levels arising from the configurations ($1s^2$) $2s^2$ sp^6, $2s^22p^5$ 3l,$2s^22p^5$ 4l, $2s^12p^6$ 3l,and $2s^12p^6$ 4l where *l = s,p,d, and f* are calculated with the J–J atomic notation . The calculations have been obtained by FAC [28]. The bound states of the atomic system were calculated using the configuration mixing approximation. A modified self-consistent Dirac–Fock–Slater iteration was used to derive the radial part of wavefunction for the construction of basis states.

Oscillator Strengths and Allowed transition probabilities

The equations describing the weighted oscillator strengths as well as spontaneous radiative decay rates are presented for transitions between the configurations ($1s^2$) $2s^2$ sp^6, $2s^22p^5$ 3l,$2s^22p^5$ 4l, $2s^12p^6$ 3l,and $2s^12p^6$ 4l where *l = s,p,d,f* . The weighted oscillator strengths gf_{ul} [28] are given as:

$$gf_{ul} = L^{-1}\omega(\alpha\omega)^{2L-2}S_{ul}\,, \qquad (1)$$

Where ω is the transition energy and S_{ul} is the line strength given by:

$$S_{ul} = \left| < \psi_u \,||\, O^L || \psi_l > \right|, \qquad (2)$$

where, O^L refers to the spherical multipole operator of rank L that represents the electrons' interactions with the electromagnetic field, and ψ_l and ψ_u are the initial state and final state of the transition, respectively. The weighted radiative transition probability gA_{ul} can be related to the weighted oscillator strength as follows:

$$gA_{ul} = 2\alpha^3\omega^2 gf_{ul}\,, \qquad (3)$$

The radiative decay rates were calculated within the framework of the single multipole approximation with arbitrary ranks, (i.e) the interference between different multipoles isn't considered. For these, the atomic structure program FAC was employed [28]. The redial part of single multipole operator calculated using fully relativistic expressions of Grant [29], which is

essentially for M1 transitions. However in most cases the nonrelativistic limits have good accuracy. For which, the spherical multipole operator is simply depend on the transitions energy.

Computation of gain coefficient

Firstly, XUV and soft X-ray laser emission possibility at various temperatures of plasma and plasma electron densities from plasma of Ar^{8+} ion via electron collisional pumping is investigated. The coupled rate equations [30-33] are solved to calculate the reduced population densities.

$$N_j\left[\sum_{i<j} A_{ji} + N_e\left(\sum_{i<j} C_{ji}^{d} + \sum_{i>j} C_{ji}^{e}\right)\right] = N_e\left(\sum_{i<j} N_i C_{ij}^{e} + \sum_{i>j} N_i C_{ij}^{d}\right) + \sum_{i>j} N_i A_{ij} \quad (4)$$

where N_j is the population of level j, A_{ji} is the allowed transition probability from level j to level i, C^{d}_{ji} is the electron collisional de-excitation rate coefficient, and C^{e}_{ji} is the electron collisional excitation rate coefficient, while C^{d}_{ji} is related to C^{e}_{ji} by [34-35].

$$C_{ji}^{d} = C_{ij}^{e}[\frac{g_i}{g_j}]\exp[\frac{\Delta E_{ji}}{KT_e}] \quad (5)$$

Where g_j and g_i refer to the statistical weights of upper and lower levels respectively. Based on the effective collision strengths γ_{ij}, electron impact excitation rates can be given by:

$$C_{ij}^{e} = \frac{8.6287\times10^{-6}}{g_i T_e^{1/2}}\gamma_{ij}\exp\frac{E_{ij}}{KT_e} \quad (6)$$

The effective collision strength is obtained as a function of electron temperature by integrating the collision strength Ω over a maxwellian distribution of electron velocities as[36]

$$\gamma_{lu}(T_e) = \int_0^{\infty} \Omega(E) exp\frac{-E_u}{KT_e}\, d(\frac{E_u}{KT_e}) \quad (7)$$

here E_u is the the electron energy after collision. The collision strength is a dimensionless quantity, and related to the collision cross section by

$$\Omega_{lu}(E) = K_l^2 g_l \sigma_{lu}(\pi a_0^2) \qquad (8)$$

where K_l is the incident electron energy, g_l is the statistical weight of the initial level l, and σ_{lu} is the collision cross section in units of πa_0^2

The density of actual population N_J of the j^{th} level was obtained using the following identity [32],

$$N_J = N_j \times N_I \qquad (9)$$

Where N_I is the amount of ions that can reach the ionization stage *I*. N_I is calculated by:

$$N_I = f_I \frac{N_e}{Z_{avg}} \qquad (10) \quad ,$$

where f_I is the abundance of fractions of the Ne- like ionization stages , N_e is the electron density, and Z_{avg} is the average degree of ionization. Since the fractional populations calculated from Eq. (4) are normalized such that,

$$\sum_{J=1}^{89} \left(\frac{N_J}{N_I}\right) = 1 \qquad (11) \,,$$

where's 89 is the number of the whole levels of the ion in consideration. Thereby, the reduced population of upper levels (N_u/g_u) and lower levels (N_l/g_l) can be calculated. In the lasant ion plasma, the pumped quanta will be transmitted to other levels by collision after application of electron collisional pumping mechanism; If a population inversion has been confirmed to be a positive gain through F>0, this will cause the occurrence of population inversions among the lower and upper levels [37].

$$F = \frac{g_u}{N_u}\left[\frac{N_u}{g_u} - \frac{N_l}{g_l}\right] \qquad (12)$$

Where N_l/g_l and N_u/g_u are the reduced populations of the lower level and upper level respectively.

The dominant broadening mechanism under the plasma conditions conductive to X-ray lasing is Doppler broadening. The condition we chose are Ti = 2/3 Te (where Ti and Te are the ion and electron temperature respectively). Finally, the gain coefficients (α) of the different transitions in the Ar^{8+} ion has to be considered;

$$\alpha = \frac{\lambda_{lu}^3}{8\pi}\left(\frac{M}{2\pi K T_i}\right)^{1/2} A_{ul} N_u F \qquad (13)$$

where λ_{lu} refers to the transition wavelength measured in *cm*, *M* is the ion mass, *K* is Boltzmann constant, T_i is the ion temperature in Kelvin and *u,l* are the upper and lower transition levels respectively. The gain coefficient is expressed in terms of the upper state density (N_u), this quantityis dependent on how the upper state is populated, as well as on the density of the initial source state. The source state is often regarded as the ground state for the particular ion.

Results and Discussion

Atomic Structure

The calculated values of the energy levels of a Ne-like Ar contributed in production of soft x-ray laser radiation were presented in Table 1. A comparison with the other experimental data is also presented [38].

The calculated energy levels showed, in general, a fairly good accord with the other experimental data. This is an indication of the proper choice of the radial wavefunctions. The radiative transitions probabilities and weighted oscillator strengths values for possible laser transitions are presented in Table 2.

Levels Population and Gain Coefficients

The reduced population densities are evaluated for 89 fine structure levels arising from $(1s^2)\ 2s^2\ sp^6$ and 88 fine-structure levels contained in the configurations $2s^22p^5\ 3l$, $2s^22p^5\ 4l$, $2s^12p^6\ 3l$, and $2s^12p^6\ 4l$ where l = s,p,d,f configurations that emit coherent radiation in the XUV and soft x-ray spectral regions. A MATLAB developed algorithm is used for solving the coupled rate

Eq.(4) simultaneously. The relation between the reduced populations results and the electron densities at three different plasma temperatures (105, 210, 315 eV) are drawn in Figs. (1 to 3) for Ar IX ion. The processes of electron collisions between all levels and the rate of spontaneous radiative decay were taken into account. The way of behaving of level populations shows in general that the reduced population density is proportional to the electron density at low electron densities, (i,e) excitation to an excited state is immediately followed by radiative decay. Moreover, excited levels' collisional mixing can be disregarded, however at high electron densities (> 6×10^{19}), the radiative decay to all the levels will be of no account compared to depopulations by collision and all the level populations become approximately constant independent of the electron density as shown in Figs. 1 to 3.

Table 1. Calculated Energy levels and fine structure splitting (in eV) For Ar IX

index	Level	J^{π}	$E_{cal.}$	$E_{[37]}$	Deviation(%)
3	$2p_{3/2}\,3s_{1/2}$	1^{o}	250.8	252.07	0.52
5	$2p_{1/2}\,3s_{1/2}$	1^{o}	253.2	254.38	0.47
6	$2p_{3/2}\,3p_{3/2}$	1^{e}	265.0	266.48	0.57
9	$2p_{3/2}\,3p_{1/2}$	1^{e}	268.6	269.88	0.46
11	$2p_{1/2}\,3p_{1/2}$	1^{e}	270.2	271.43	0.45
14	$2p_{1/2}\,3p_{3/2}$	1^{e}	271.1	271.43	0.13
28	$2s_{1/2}\,3s_{1/2}$	1^{e}	328.2	325.23	-0.89
31	$2p_{3/2}\,4s_{1/2}$	1^{o}	333.8	335.28	0.44
32	$2p_{1/2}\,4s_{1/2}$	0^{o}	335.6	------	
37	$2p_{3/2}\,4p_{3/2}$	1^{e}	340.8	341.61	0.22
39	$2p_{3/2}\,4p_{3/2}$	0^{e}	342.1	------	
40	$2p_{1/2}\,4p_{1/2}$	1^{e}	342.5	342.32	-0.05
43	$2s_{1/2}\,3p_{1/2}$	0^{o}	346.1	------	
46	$2p_{1/2}\,4p_{1/2}$	0^{e}	346.8	------	
47	$2s_{1/2}\,3p_{3/2}$	1^{o}	347.5	345.54	-0.58
48	$2p_{3/2}\,4d_{3/2}$	0^{o}	348.5	349.89	0.40
77	$2s_{1/2}\,4s_{1/2}$	0^{e}	412.5	------	
78	$2s_{1/2}\,4p_{1/2}$	0^{o}	418.0	------	

Table 2: Wavelength, weighted oscillator strength and transition probabilities.

i	*j*	Transition	*λ(nm)*	*gf*	$A_{ji}(sec)^{-1}$
6	32	$(2p_{1/2}\ 4s_{1/2})_0 \rightarrow (2p_{3/2}\ 3p_{3/2})_1$	17.5	1.69E-02	3.65E+09
9	32	$(2p_{1/2}\ 4s_{1/2})_0 \rightarrow (2p_{3/2}\ 3p_{1/2})_1$	18.5	4.05E-02	7.89E+09
11	32	$(2p_{1/2}\ 4s_{1/2})_0 \rightarrow (2p_{1/2}\ 3p_{1/2})_1$	18.96	1.04E-01	1.94E+10
14	32	$(2p_{1/2}\ 4s_{1/2})_0 \rightarrow (2p_{1/2}\ 3p_{3/2})_1$	19.2	6.36E-02	1.15E+10
3	39	$(2p_{3/2}\ 4p_{3/2})_0 \rightarrow (2p_{3/2}\ 3s_{1/2})_1$	13.5	3.28E-02	1.19E+10
6	43	$(2s_{1/2}\ 3p_{1/2})_0 \rightarrow (2p_{3/2}\ 3p_{3/2})_1$	15.3	5.84E-02	1.67E+10
9	43	$(2s_{1/2}\ 3p_{1/2})_0 \rightarrow (2p_{3/2}\ 3p_{1/2})_1$	16.0	1.86E-01	4.85E+10
14	43	$(2s_{1/2}\ 3p_{1/2})_0 \rightarrow (2p_{1/2}\ 3p_{3/2})_1$	16.5	5.94E-02	1.45E+10
5	46	$(2p_{1/2}\ 4p_{1/2})_0 \rightarrow (2p_{1/2}\ 3s_{1/2})_1$	13.2	2.94E-02	1.12E+10
6	48	$(2p_{3/2}\ 4d_{3/2})_0 \rightarrow (2p_{3/2}\ 3p_{3/2})_1$	14.8	3.60E-02	1.09E+10
28	78	$(2s_{1/2}\ 4p_{1/2})_0 \rightarrow (2s_{1/2}\ 4s_{1/2})_1$	13.8	5.61E-02	1.96E+10
31	77	$(2s_{1/2}\ 4s_{1/2})_0 \rightarrow (2p_{3/2}\ 4s_{1/2})_1$	15.8	1.34E-01	3.58E+10
37	78	$(2s_{1/2}\ 4p_{1/2})_0 \rightarrow (2p_{3/2}\ 4p_{3/2})_1$	16.0	1.10E-01	2.86E+10
40	78	$(2s_{1/2}\ 4p_{1/2})_0 \rightarrow (2p_{1/2}\ 4p_{1/2})_1$	16.4	8.20E-02	2.03E+10
47	77	$(2s_{1/2}\ 4s_{1/2})_0 \rightarrow (2p_{3/2}\ 3p_{3/2})_1$	19.1	1.68E-01	3.07E+10

The maximum values of population inversion are reached when the rate of the collisional deexcitation of electrons for the upper level is comparable to the rate of radiative decay for this level [32, 39].

Positive gain will be found in laser medium as a result of population inversion. The gain coefficients for the Doppler broadening of various transitions in the Ar IX ion were calculated using Eq. (11). The gain coefficients in cm^{-1} for those transitions are drawn in Figs. (4 to 6).

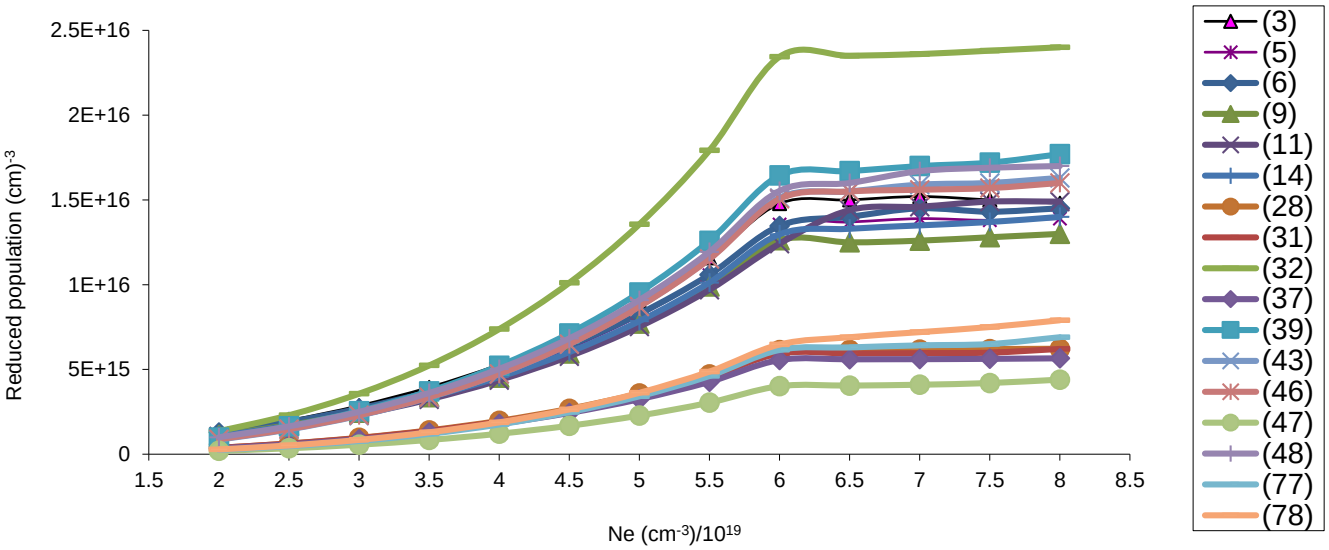

Fig. (1): Reduced population of Ar IX levels after electron collisional pumping as a function of the electron density at temperature 105 eV.

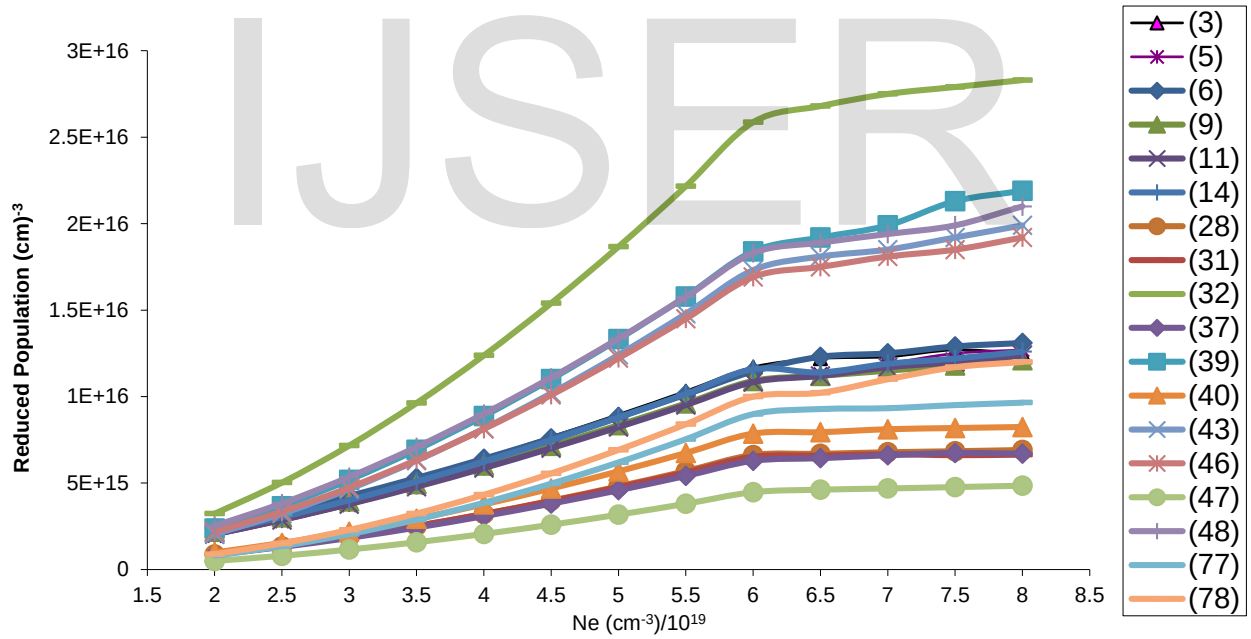

Fig. (2): Reduced population of Ar IX levels after electron collisional pumping as a function of the electron density at temperature 210 eV.

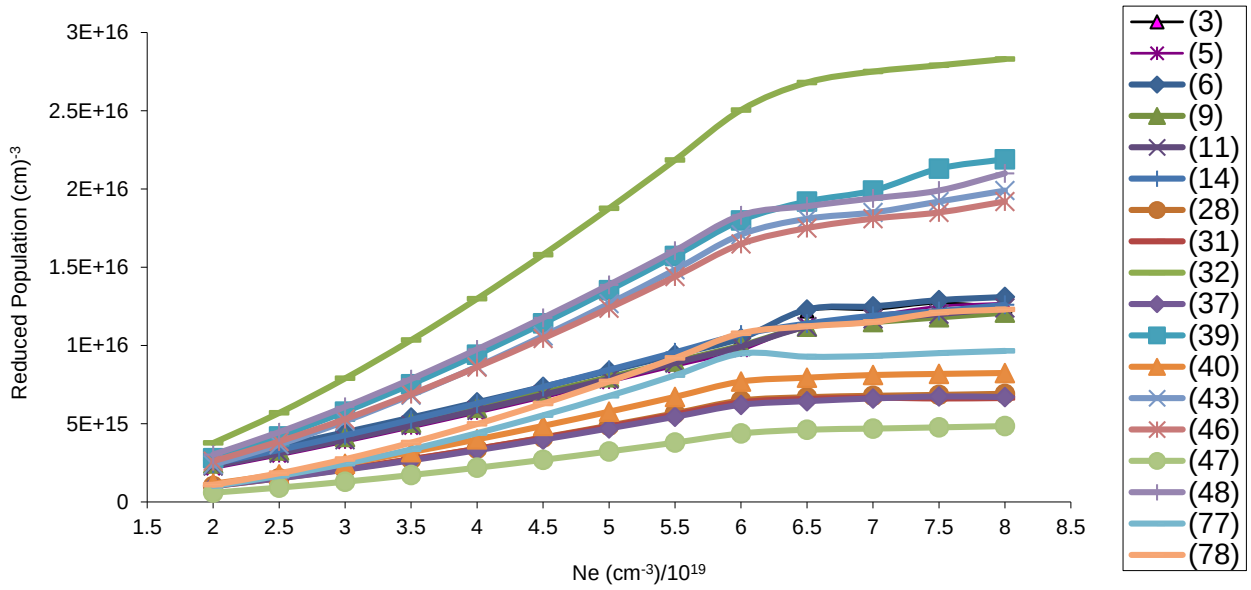

Fig. (3): Reduced population of Ar IX levels after electron collisional pumping as a function of the electron density at temperature 315 eV.

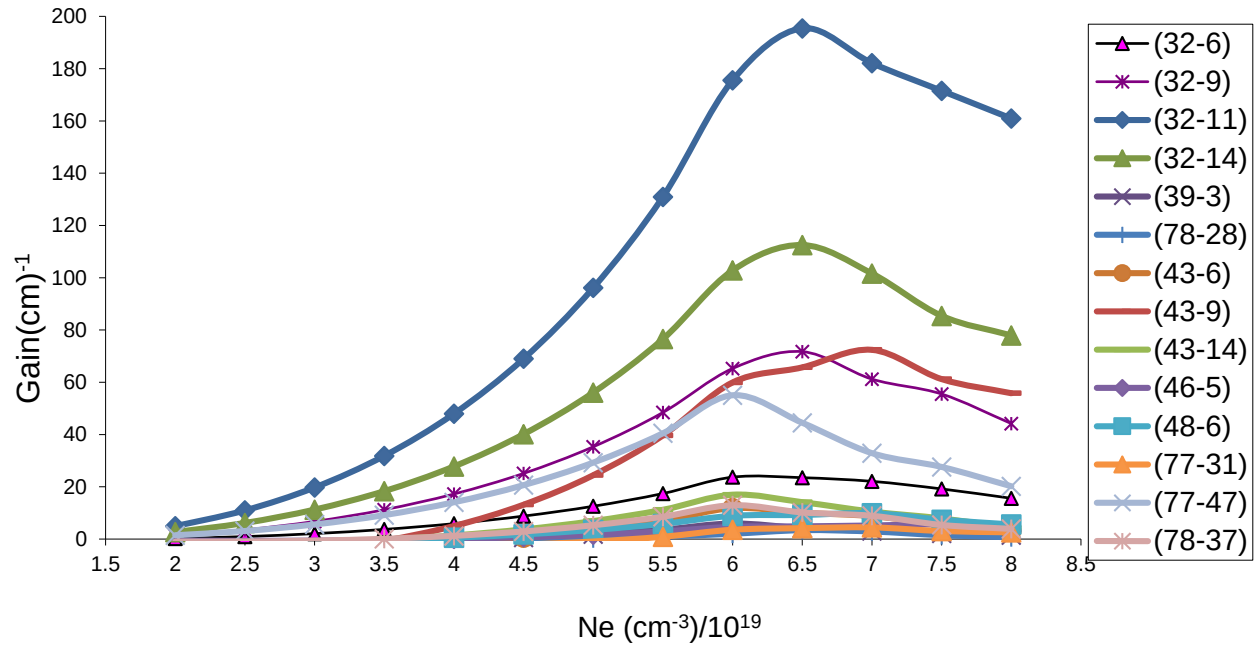

Fig. (4): Gain coefficient of possible laser transitions against electron density at temperature 105 eV in Ar IX.

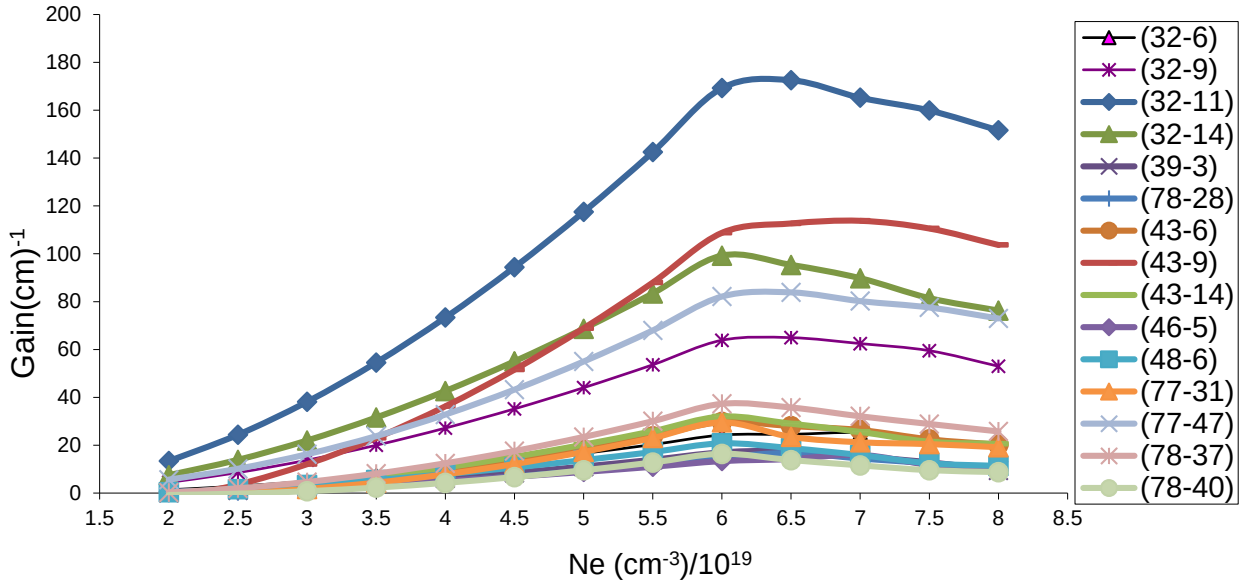

Fig. (5): Gain coefficient of possible laser transitions against electron density at temperature 210 eV in Ar IX.

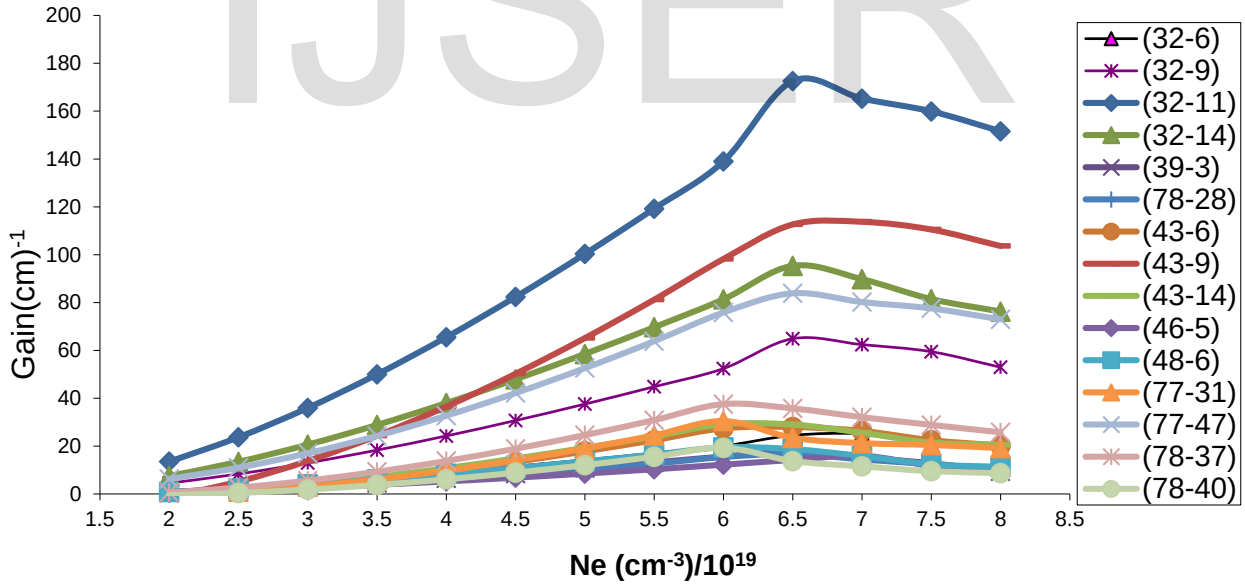

Fig. (6): Gain coefficient of possible laser transitions against electron density at temperature 1.5 eV in Ar IX.

It can be observed that, population inversions take place for several transitions in the Ar IX ion, however, the largest gain takes place in $(2p_{1/2}\ 4s_{1/2}\ )_0 \rightarrow (2p_{1/2}\ 3p_{1/2}\ )_1$ (32→11) transition at

wavelength 18.69 nm at three electron temperatures. The population inversion occurs as a result of strong monopole excitation from the $2p^6$ ground state to the $2p^53p$ configuration meanwhile the radiative decay of the $2p^53p$ level to the ground level is forbidden, the $3p^54s$ level decays so fast to the ground level. Thus, using plasmas that were created by optical lasers as a lasting medium, these soft x-ray lasers wavelengths were produced. It has to be mentioned that, for experimental conditions (electron densities and electron temperatures) that are typical of high-density plasma sources laboratories, it is possible to create such laser from produced plasmas, and a quasistationary population inversion between many levels in Ar IX ion could occurred. From our calculations, one can conclude that under appropriate conditions, large laser gain in the neon like Ar IX ion for these transitions in the regions of XUV and soft X-ray of the spectrum can be achieved.

Conclusion

The analysis presented in this study shows that the collisional pumping of electrons is appropriate for producing population inversion and for offering the potential for laser radiation in the spectral region between 1 and 30 nm from Ar IX ion as well. These short lasers wavelengths can be achieved under appropriate conditions of pumping power as well as electron density. For the ion under study (Ar IX ion), if the positive gain obtained previously for some transitions in together with the evaluated parameters could be achieved practically, a successful low-cost electron collisional pumping of soft X-ray and XUV lasers can be achieved for various applications.

Acknowledgments

The author thank Prof. Wessameldin S. Abdelaziz. National Institute of Laser Enhanced Sciences, Cairo University, Prof. Tharwat M. Elsherbini, Physics department. Faculty of Science, Cairo University and Prof. Maram T.H. Abou Kana, National Institute of Laser Enhanced Sciences, Cairo University, Cairo University for supporting me throughout this study.

References

[1] Matthews DL, Hagelstein PL, Rosen MD, Eckart M, Ceglio NM, Hazi, AU, et al. Demonstration of a Soft X-Ray Amplifier Phys. Rev. Lett. 1985; 54:110.

[2] Suckewer S, Skinner CH, Milchberg H, Keane C, Voorhees D. Amplification of Stimulated soft x-ray emission in a confined plasma column Phys. Rev L ett. 1985**;** 55: 1753.

[3] Rocca JJ, Shlyaptsev V, Tomasel FG, Cortázar OD, Hartshorn D, Chilla JLA. Demonstration of a Discharge Pumped Table Top Soft X-Ray Laser. Phys. Rev L ett**.** 1994; 73- 2192.

[4] Alessi D, Wang Y, Luther BM, Yin L, Martz DH, Woolston MR, Liu Y, Berrill M, and Rocca JJ. Efficient Excitation of Gain-Saturated Sub-9-nm-Wavelength Tabletop Soft-X-Ray Lasers and Lasing Down to 7.36 nm. Phys. Rev. X **1**, 2011; 021023.

[5] Popmintchev T, Chen MC, Popmintchev D, Arpin P, Brown S, Ališauskas S, Andriukaitis G, Balčiunas T, Mücke OD, Pugzlys A, Baltuška A, Shim B, Schrauth SE, Gaeta A, García CH, Plaja L, Becker A, Becker AJ, Murnane MM, Kapteyn HC. Bright Coherent Ultrahigh Harmonics in the keV X-ray Regime from Mid-Infrared Femtosecond Lasers. Science 2012; 336- 1287.

[6] Kukhlevsky SV, Ritucci A, Kozma LZ; Kaiser J, Shlyaptsev A, Tomassetti G, et al. Atomic Model Calculations of Gain Saturation in the 46.9 nm Line of Ne- like Ar Contrib. Plasm. P hys.2002; 42:109-18.

[7] Heinbuch S, Grisham M, Martz D, Rocca JJ. Demonstration of a desk-top size high repetition rate soft x-ray laser Opt. Express **2005**; 1**3:**4050.

[8] Namba S, John C, Morishita T, Kubo N, Kishimoto M, Hasegawa N, Nishikino M. Observation of gain coefficients of 15.47 nm Li-like Al soft x-ray laser in a recombining plasma pumped by a compact YAG laser. High Energy Density Physics, 2020; 36:100790.

[9] Abdelaziz WS, El Sherbini TM. Reduced population and gain coefficient calculations for soft X-ray laser emission from Eu^{35+}.Optics & Laser Technology 2010; 42: 699.

[10] Sayed MA, Allam SH, El-Sherbini TM. Laser gain calculations for soft X-ray and XUV radiation emitted from copper-like ions by electron collisional pumping. *Canadian Journal of Physics* 2016; 94(10): 967.

[11] King RE, Pert GJ, McCabe SP, Simms PA, MacPhee AG, Lewis CLS, et al. Saturated X-Ray Lasers at 196 A and 73 A Pumped by Picosecond Travelling Wave Excitation. Phys. Rev. A 2001; 64:053810.

[12] Tomsel FG, Rocca, JJ, Shlyaptsev VN, Macchietto CD. Lasing at 60.8 nm in Ne-Like Sulfur Ions in Ablated Material Excited by a Capillary Discharge. Phy. Rev. A 1997; 55:1437.

[13] Healy SP, Janulewicz KA, Pert GJ. Short Wavelength Lasing on Collisionally Pumped, Highly Excited 2s Hole States of Neon Like Ions in Performed Plasmas Irradiated with Picosecond Pulses. Optics Communications, 1997; 144: 24.

[14] Simms PA, McCabe S, Pert GJ. Comparison of Neon Like Germanium Inner Shell and Nickel Like Gadolinium at 62 Å and 66 Å by Picosecond Heating of a Performed Plasma. Optics Communications, 1998;153: 164.

[15] Abdelaziz WS. Calculation of Atomic Data and Gain Coefficient for XUV & Soft X-Ray Laser Emission from Ge XXIII. Optics and Photonics Journal 2014;4:246.

[16] LiuY, Seminario M, Tomasel FG, Chang C, Rocca JJ, Attwood DT. Achievement of essentially full spatial coherence in a high-average-power soft-x-ray laser Phys. Rev. A 2001; 63: 033802.

[17] Hammarsten EC, Szapiro B, Jankowska E, Filevich J, Marconi MC, Rocca JJ. Soft X-ray laser diagnostics of exploding aluminum wire plasmas, Appl Phys B 2004; 78:933.

[18] Mocek T, Rus B, Präg AR, Kozlová M, Jamelot G, Carillon A, Ros D. Beam properties of a deeply saturated, half-cavity zinc soft-x-ray laser Journal of theOptical Society of America B,2003; 20(6):1386.

[19] Mocek T, Rus B, Stupka M, Kozlová M, Präg AR, Polan J, et al. Focusing a multimillijoulesoft x-ray laser at 21nm Appl. Phys. Let**t.** 2006; 9: 051501.

[20] Mocek T, Rus B, Kozlová M, Polan J, Homer P, Jakubczak K, et al. Plasma-based X-ray laser at 21 nm for multidisciplinary applicationsEur. Phys. J. D 2009**;** 54: 439.

[21] Rus B, Mocek T, Präg AR, Kozlová M, Jamelot G, Carillon A, et al. Multimi-joule highly coherent x-ray laser at 21 nm operating in deep saturation through double-pass amplification Phys. Rev. A 2002**;** 66: 063806.

[22] Ahmad M, El-Maaref AA, Abdel-Wahab E, Allam S. Population Inversion and X-Ray Laser Gain by Electron Impact Excitation of Ni-Like Tin. American Journal of Optics and Photonics.2015; 3(1): 17.

[23] Edwards MH, Whittaker DS, Tallents GJ, Mistry P, Pert GJ, Rus B, et al. Laser-Ablation Rates Measured Using X-Ray Laser Transmission Phys. Rev. Lett. 2007; 99: 195002.

[24] Pestehe SJ, Farzan M A. coupled gain calculation and output characteristics of the two Ne-like 2s and 2p hole X-ray laser lines Journal of Quantitative Spectroscopy& Radiative Transfer 2006; 98:309.

[25] Yoneda H, Inubushi Y, Nagamine K, Michine Y, Ohashi H, Yumoto H, Yamauchi K, Mimura H, Kitamura H, Katayama T, Ishikawa T, Yabashi M. Atomic inner-shell laser at 1.5-ångström wavelength pumped by an X-ray free-electron laser. Nature 2015; 524: 446.

[26] Nilsen J. Modeling the gain of inner-shell X-ray laser transitions in neon, argon, and copper driven by X-ray free electron laser radiation using photo-ionization and photo-excitation processes. Matter and Radiation at Extremes 2016;1: 132

[27] Zhang H, Li K, Yan J, Deng H, Sun B. Atomic inner-shell radiation seeded free-electron lasers. PHYSICAL REVIEW ACCELERATORS AND BEAMS 2018;21: 070701.

[28] Gu M.F, Indirect X-Ray Line-Formation Processes in Iron L-Shell Ions. The Astrophysical Journal 2003; 582(2): 1241.

[29] Grant I.P, Gauge invariance and relativistic radiative transitions. J. Phys. B 1974; 7: 1458.

[30] Feldman U, Bhatia A K, Suckewer S. Short wavelength laser calculations for electron pumping in neon-like krypton (Kr XXVII) J. Appl. Phys. 1983; 54 (5): 2188.

[31] Feldman U, Seely JF, Doschek GA, Bhatia AK. 3s–3p laser gain and x-ray line ratios for the carbon isoelectronic sequence J. appl. Phys. 1986; 59(12): 3953.

[32] Feldman U, Doschek G A, Seely JF, Bhatia AK. Short wavelength laser calculations for electron pumping in Be I and B I isoelectronic sequences ($18 \leq Z \leq 36$) J. appl. Phys.1985; 58(8): 2909.

[33] Feldman U, Seely JF, Bhatia AK. Scaling of collisionally pumped 3*s*-3*p* lasers in the neon isoelectronic sequence J. appl. Phys. 1984; 56(9): 2475.

[34] Chapline G, Wood L, X-ray lasers Phys. Today 1975; 28: 40.

[35] Vinogradov AV, Shlyaptsev VN. Calculations of population inversion due to transitions in multiply charged neon-like ions in the 200–2000 Å range Sov. J. Quant. Electron. 1980; 10(6): 754.

[36] Aggarwal K M, Keenan F P, Kisielius R, Norrington P H, King R E, Pert G J, Rose S J. Radiative Rates, Collision Strengths and Effective Collision Strengths for Transitions in Gd XXXVII phys. Scr. 2005; 71: 356.

[37] Sobel'man II. Introducrion to the Theory of Atomic Spectra, International Series Of Monographs In Natural Philosophy, Pergamon Press 1979; Vol. 40.

[38] Saloman EB. Energy levels and observed spectral lines of ionized argon, Ar II through Ar XVIII J. Phys. Chem. Ref. Data 2010; 39(3): 0331011.

[39] Feldman U, Seely JF, Bhatia AK. Density sensitive x-ray line ratios in the Bei, B i, and NeI isoelectronic sequences J. appl. Phys.1985; 58(11):3954.